Solar Energy Materials & Solar Cells 104 (2012) 97–101

Contents lists available at SciVerse ScienceDirect

Solar Energy Materials & Solar Cells

journal homepage: www.elsevier.com/locate/solmat

Anomalous *IV*-characteristics of a GaAs solar cell under high irradiance

G.M.M.W. Bissels *, M.A.H. Asselbergs, G.J. Bauhuis, P. Mulder, E.J. Haverkamp, E. Vlieg, J.J. Schermer

Radboud University Nijmegen, Institute for Molecules and Materials, Heyendaalseweg 135, 6525 AJ Nijmegen, The Netherlands

ARTICLE INFO

Article history:
Received 15 July 2011
Received in revised form
27 April 2012
Accepted 1 May 2012
Available online 31 May 2012

Keywords:
Back surface field
Energy barrier
Temperature dependence
Irradiance dependence
Maximum power point voltage

ABSTRACT

High irradiance *IV*-measurements on a CPV GaAs cell with an $(Al_{0.4}Ga_{0.6})_{0.52}In_{0.48}P$ back surface field revealed some unusual characteristics. With increasing irradiance, an anomaly appeared in the high voltage section of the *IV*-curve. The anomaly disappeared at sufficiently high temperatures. Because the layer structure of the studied GaAs solar cell is not uncommon, this effect could be more widespread among concentrator cells and is, therefore, of interest to the CPV community. It was demonstrated that the effect is due to a back surface field-related energy barrier and can be avoided by using an $Al_{0.2}Ga_{0.8}As$ back surface field with a higher doping level. The behavior of the anomaly as a function of temperature seems to be in agreement with the mechanism of thermionic emission of current over an internal energy barrier. This mechanism, however, does not explain the irradiance-dependent occurrence of the anomaly.

1. Introduction

Over the years, the Radboud University Nijmegen (RU) has successfully developed the epitaxial lift-off (ELO) process [1,2]. It involves the separation of a single crystalline III–V thin film cell structure from the substrate it was deposited on, by selective wet etching of an intermediate release layer. The cell structure is transferred to a cheap foreign carrier and further processed into a high-efficiency solar cell, while the substrate can be reused for the deposition of a new cell structure. One of the advantages that this brings is a decrease in the amount of required III–V materials up to a factor of 100 and, therefore, a significant reduction in the cost of photovoltaic energy. The ELO process was developed utilizing single-junction GaAs solar cells, and during this development the cell design was optimized as well. This resulted in a crystal layer structure with an AlInP window and $(Al_{0.4}Ga_{0.6})_{0.52}In_{0.48}P$ back surface field (BSF) that yielded a world record GaAs cell efficiency of 26.1 % in 2009 [3,4].

In the present work the performance of the above described GaAs cell structure is studied under high irradiance levels. For this purpose a small specimen with a high grid coverage was produced. The *IV*-characteristics of this cell under irradiation levels ranging from 1 to 125 suns and operating temperatures between 5 and 80 °C are described and compared to that of a similar cell having an $Al_{0.2}Ga_{0.8}As$ instead of an $(Al_{0.4}Ga_{0.6})_{0.52}In_{0.48}P$ BSF. In this temperature range, the open circuit voltage V_{oc} should decrease approximately linear with increasing temperature, since

$$\frac{dV_{oc}}{dT} \approx \frac{V_{oc} - E_{g0}/q}{T} - \frac{\gamma k}{q}, \quad (1)$$

as derived by Green [5]. Here T is the absolute temperature, E_{g0} is the bandgap at $T = 0$ K, γ is an empirical parameter independent of T, k is Boltzmann's constant and q is the elemental charge. The approximately linear decrease of V_{oc} with increasing T that this theory predicts has also been experimentally confirmed, and the literature value for the temperature coefficient of a GaAs solar cell is -2.0 mV/°C at room temperature [6]. A similar derivation for the temperature dependence of the voltage at maximum power point V_{mp} leads to

$$\frac{dV_{mp}}{dT} \approx \frac{V_{mp} - E_{g0}/q}{T} - \frac{\gamma k}{q}, \quad (2)$$

so for the above-mentioned temperature range V_{mp} should decrease approximately linearly with increasing T as well.

2. Experimental

The solar cells were grown by low-pressure MOCVD on 2-in. GaAs wafers with a (100) 2° off to [110] orientation. Arsine and phosphine were used as group-V source gases, trimethyl-gallium, trimethyl-indium and trimethyl-aluminium as group-III precursors. For n- and p-type doping, disilane and diethylzinc were used, respectively. The growth took place at temperatures between 600 and 700 °C and at a pressure of 20 mbar.

In this study two different cell structures are compared. The cell referred to as cell A has the layer structure shown in Fig. 1,

* Corresponding author. Tel.: +31 24 3652586.
E-mail address: G.Bissels@science.ru.nl (G.M.M.W. Bissels).

0927-0248/$ - see front matter © 2012 Elsevier B.V. All rights reserved.
http://dx.doi.org/10.1016/j.solmat.2012.05.001

300 nm	cap	n++ GaAs
30 nm	window	n AlInP
150 nm	emitter	n GaAs
2000 nm	base	p GaAs
50 nm	BSF	p $(Al_{0.4}Ga_{0.6})_{0.52}In_{0.48}P$
300 nm	buffer	p GaAs
350 μm	substrate	p GaAs

Fig. 1. Layer structure of cell A. The doping concentration of the base and BSF is 1.0 and $2.3\times10^{17}\,cm^{-3}$ respectively. Cell B has a similar structure, but with a $7.0\times10^{18}\,cm^{-3}$ doped $Al_{0.2}Ga_{0.8}As$ BSF.

with doping concentrations of 1.0 and $2.3\times10^{17}\,cm^{-3}$ for the base and BSF layers respectively. This structure is identical to the one applied in a previous study to obtain a 26.1% efficiency GaAs cell under 1 sun AM1.5G irradiation [3]. Cell B has a similar layer structure but instead of $(Al_{0.4}Ga_{0.6})_{0.52}In_{0.48}P$ it has an $Al_{0.2}Ga_{0.8}As$ BSF with a doping level of $7.0\times10^{18}\,cm^{-3}$.

Contacts were applied using e-beam evaporation, with the front contact having a square grid with a coverage of 25%, suited for high irradiance levels. The cells have an area of $4.9\times4.1\,mm^2$ as defined by a mesa etch. Cell A had a ZnS/MgF_2 anti-reflection coating deposited by e-beam evaporation, while cell B had no such coating applied. Both cells were covered by a glued glass sheet to avoid accidental damage of the cells and their wiring during examination.

ReRa's Tracer2 software in conjunction with a Keithley source-meter was used to measure the *IV*-curves, while the cells were illuminated using an Abet Sun 2000 Class A solar simulator for the 1-sun curves. For *IV*-curves under concentration, the cells were illuminated by a 1000 W continuous wave xenon light source, placed in the focal point of an ellipsoidal reflector. The irradiance at the cell surface could be adjusted by varying the position of the cell along the symmetry axis of the resulting light cone and the non-conformity of the irradiance never exceeded 2.7%. Measurements using this set up contain more noise at higher irradiances. The cell temperature was regulated using a Peltier element in combination with a water cooled heatsink. This temperature was monitored using a sensor connected next to the cell, and did not vary more than 0.2 °C during the measurement of an *IV*-curve.

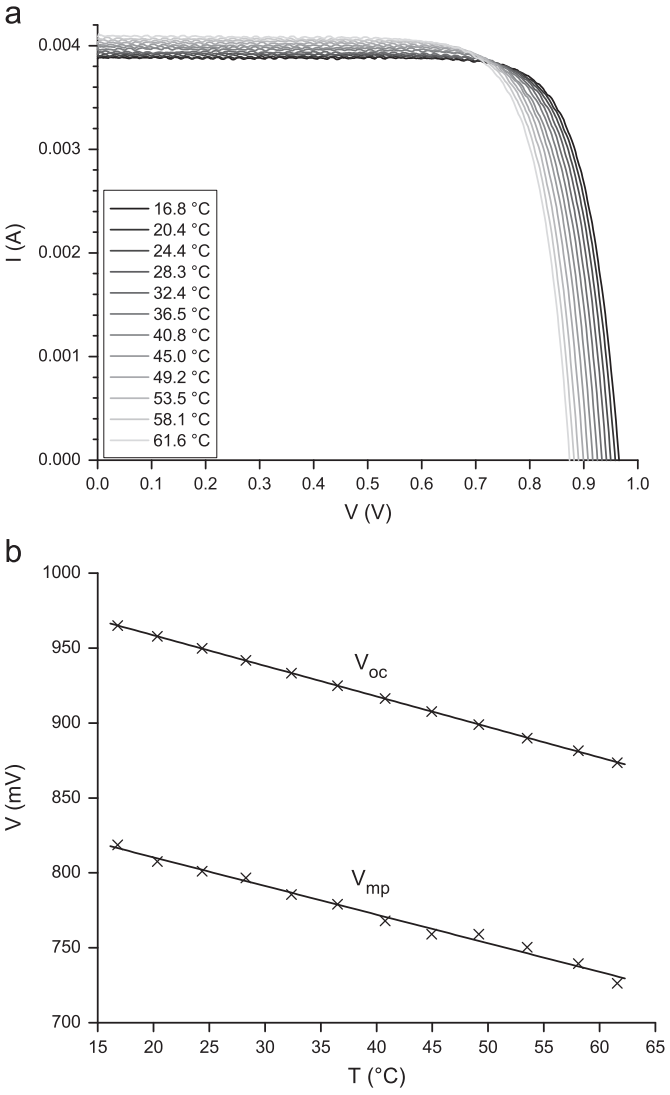

Fig. 2. (a) *IV*-curves of cell A, measured at 1 sun for a range of temperatures and (b) the associated values of V_{oc} and V_{mp} as a function of temperature. The linear fits give a slope of -2.0 mV/°C for $V_{oc}(T)$ and -1.9 mV/°C for $V_{mp}(T)$.

3. Results

At an irradiance of 1 sun, cell A generates a regular *IV*-curve. This is shown in Fig. 2a, where a series of 1-sun *IV*-curves obtained at different temperatures is displayed. In Fig. 2b the associated V_{oc} values are displayed as a function of T. One can clearly recognize the virtually linear relation predicted by Eq. (1). The linear fit perfectly matches the literature value of -2.0 mV/°C for the V_{oc} temperature coefficient [6]. Similarly, the virtually linear relation predicted by Eq. (2) can be recognized in the $V_{mp}(T)$ data displayed in Fig. 2b.

Clearly cell A follows the theoretically predicted behavior. At increasing irradiance levels, however, the *IV*-curves of the cell start to reveal an anomaly: at high voltages the current drops more rapidly than usual, only to recover just before the V_{oc} is reached, see Fig. 3. High irradiance *IV*-curves of similar cells produced at our laboratory showed signs of this anomaly as well. According to theory, the *IV*-curve of a solar cell should simply shift upwards with increasing irradiance. Apart from a small increase in V_{oc}, and a slightly smaller slope to the right of the exponential knee due to a stronger influence of the series resistance, the features of such a curve remain the same.

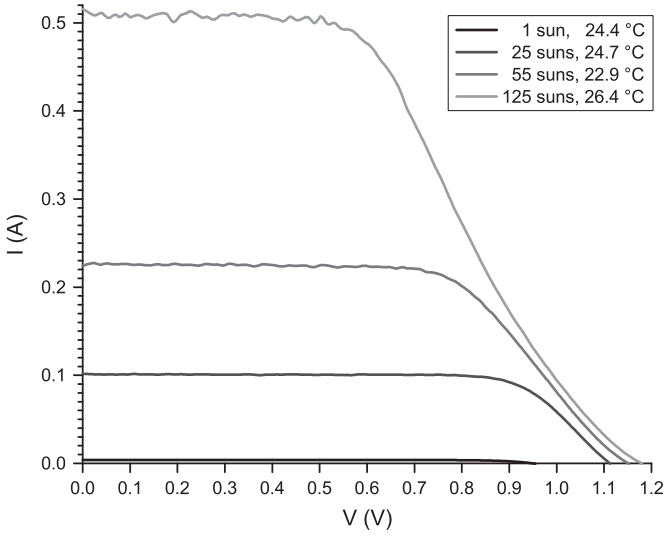

Fig. 3. Measured *IV*-curves of cell A, for a range of irradiance levels at room temperature.

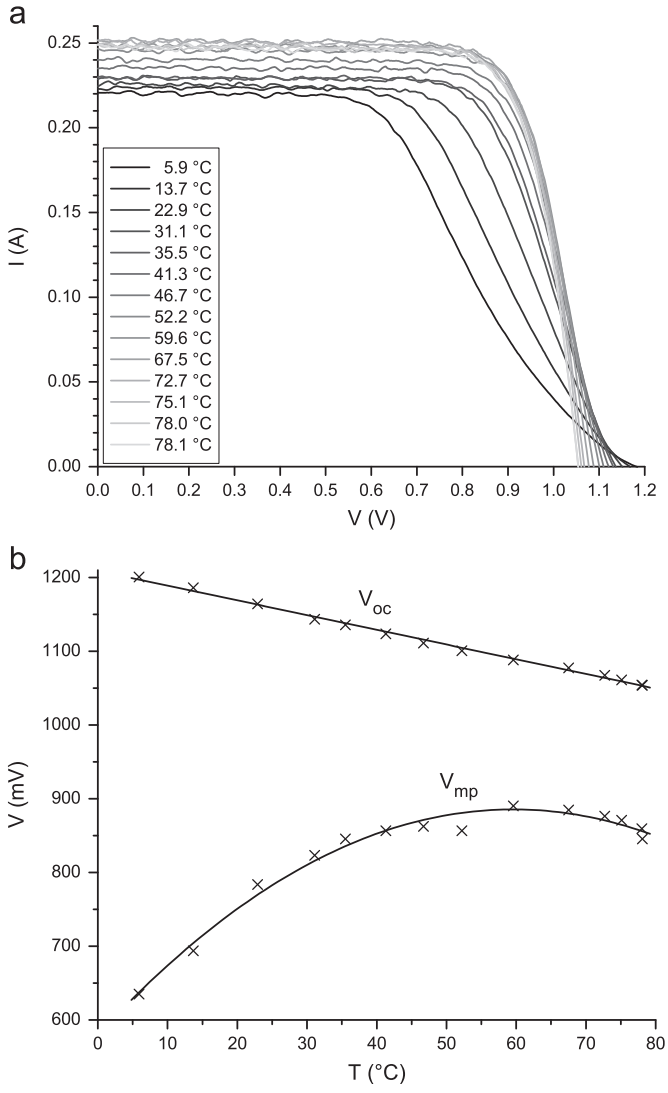

Fig. 4. (a) *IV*-curves of cell A, measured at 55 suns for a range of temperatures and (b) the associated values of V_{oc} and V_{mp} as a function of temperature. The linear fit gives a slope of -2.0 mV/°C for $V_{oc}(T)$ and the solid curve through the V_{mp} datapoints serves as a guide to the eye.

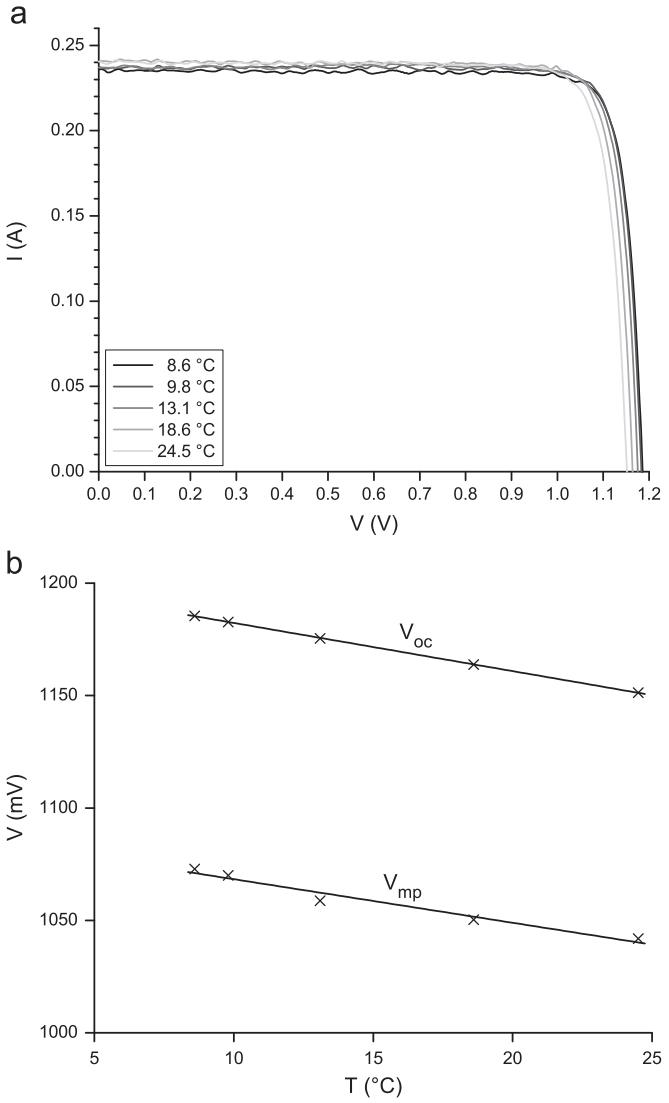

Fig. 5. (a) *IV*-curves of cell B, measured at 65 suns for a range of temperatures. Note that the fact that cell A in Fig. 4a has a higher 1-sun I_{sc} is due to the fact that cell B does not have an anti-reflection coating applied. (b) The associated values of V_{oc} and V_{mp} as a function of temperature. The linear fits give a slope of -2.1 mV/°C for $V_{oc}(T)$ and -1.9 mV/°C for $V_{mp}(T)$.

Surprisingly, the *IV*-curve converges to its characteristic shape with increasing temperature, as shown for an irradiance of 55 suns in Fig. 4a. This effect can also be observed in the associated plot of $V_{mp}(T)$ in Fig. 4b. Here, V_{mp} increases with temperature up until a turning point at about 60 °C, where the theoretically expected (linear) decrease of V_{mp} seems to get the upper hand. The behavior of V_{oc} as a function of temperature remains unaffected since the linear fit still matches the literature value of -2.0 mV/°C mentioned before.

Continuing the study of the observed effects, *IV*-curves of cell B were measured for comparison, at a similar irradiance as that which was used to obtain the curves of cell A displayed in Fig. 4. The measurements on cell B were performed for relatively low temperatures and are displayed in Fig. 5a. From this figure it is immediately clear that the anomaly observed for $T \lesssim 60$ °C in the *IV*-curves of cell A does not occur for cell B. This is supported by the plot of $V_{mp}(T)$ in Fig. 5b, which follows the theoretically expected linear behavior, already at low temperatures.

4. Discussion

The anomalies in the high irradiance *IV*-curves displayed in Fig. 3 indicate the presence of an energy barrier in cell A. The *IV*-characteristic of this barrier can be derived from the measured *IV*-curves, by assuming that these are superpositions of the *IV*-characteristics of the barrier and that of a regular cell [7]. This principle is illustrated for the 55 suns case at room temperature in Fig. 6a. The figure shows that the resulting energy barrier characteristic resembles that of a diode with a low forward voltage drop, oppositely connected to the normal solar cell. Fig. 6b contains the 55 suns *IV*-characteristics of the energy barrier at the entire investigated temperature range, obtained in the same fashion. Like Fig. 4a, it demonstrates that the energy barrier disappears with increasing temperature, since the slope increases with temperature while the forward voltage drop is independent of temperature, because $V_{oc}(T)$ of the measured *IV*-curves follows the theoretically expected behavior. This is opposite to the regular temperature dependence of a diode, in which the forward voltage drop changes with temperature, while the slope remains virtually unaffected. In fact, the observed temperature dependence of the energy barrier more closely resembles a decrease of a diode's internal series resistance with increasing temperature.

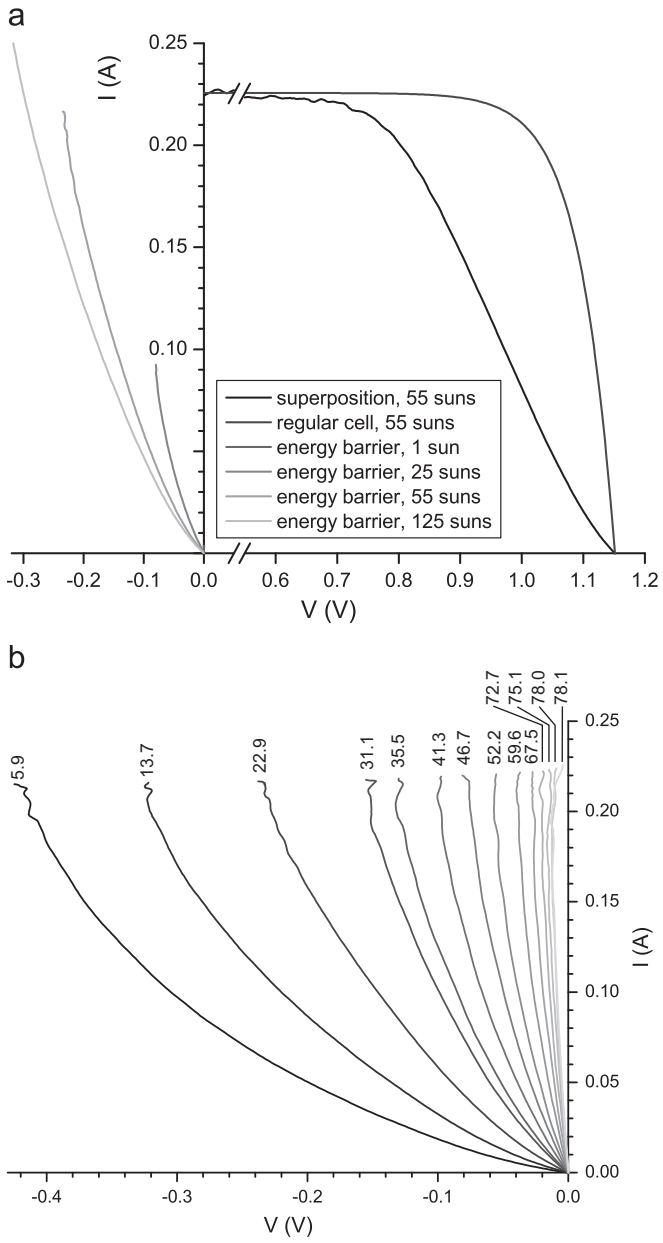

Fig. 6. (a) Energy barrier *IV*-characteristics of cell A, for a range of irradiance levels at room temperature. The 1-sun energy barrier is not clearly visible since it virtually overlaps the *y*-axis and only runs to about 0.004 A. As an example of how the energy barrier at an irradiance of 55 suns was determined, the *IV*-curve of cell A measured at 55 suns and room temperature ('superposition') and its *IV*-curve had the anomaly not been present ('regular cell') are also shown. The 'regular cell' curve was generated using the I_{sc} and V_{oc} values of the measured curve, along with fit parameters which gave a good match for the 1-sun curve of cell A at room temperature. (b) Energy barrier *IV*-characteristics of cell A, for a range of temperatures at an irradiance of 55 suns, obtained in the same fashion. Temperatures are given in °C.

The observed anomaly in the *IV*-characteristics of cell A might be related to a Schottky barrier at the metal/semiconductor interface. This, however, is highly unlikely because the anomaly has been observed in high irradiance *IV*-curves of similar cells produced at our laboratory, but not in those of cell B. Therefore, a much more likely candidate for the energy barrier in cell A is the ~430 meV valence band offset that the holes have to overcome in crossing the p-GaAs/p-$(Al_{0.4}Ga_{0.6})_{0.52}In_{0.48}P$ base/BSF heterojunction [8]. Galiana et al. have demonstrated that the barrier height of their GaAs cell's p-GaAs/p-GaInP base/BSF heterojunction of ~300 meV can be lowered to ~90 meV without a reduction of the quantum efficiency at long wavelengths, by replacing GaInP with $Al_{0.2}Ga_{0.8}As$ [9]. For this reason we produced cell B, which is similar to cell A except that the BSF now consists of $Al_{0.2}Ga_{0.8}As$ instead of $(Al_{0.4}Ga_{0.6})_{0.52}In_{0.48}P$ which also allows for a higher doping concentration. As shown in Fig. 5, *IV*-curves of cell B measured at low temperatures and a high irradiance show no sign of the anomaly observed for cell A. This indicates that it is in fact the valence band energy barrier and/or the increase in BSF doping concentration which are/is responsible for the observed effects. It also qualitatively agrees well with recently reported findings of Olson et al. [10]. Their performance simulations of a GaAs solar cell under high irradiance revealed that the fill factor decreases with increasing valence band offset and decreasing hole concentration. In addition, they present experimentally obtained high irradiance *IV*-curves of GaAs cells with a range of GaInP BSF doping levels. With decreasing doping level these curves increasingly show anomalies that are very similar to those described in the present work. The combined information from the current study and that of Olson et al. suggests that the anomalies will occur for any GaAs cell with an insufficiently doped, lattice-matched AlGaInP compound BSF under high irradiance, since GaInP is the configuration with the smallest bandgap.

Generally, the current transport across the base/BSF energy barrier is thought to be governed by thermionic emission [10,11]. The theory predicts the current to increase exponentially with temperature at a fixed bias voltage and this is indeed what is found for the energy barrier curves displayed in Fig. 6b. However, the theory does not predict an irradiance dependence of the energy barrier's *IV*-characteristic. Nevertheless, the presence of such a dependency is clear from the fact that the energy barrier curves as obtained for different irradiances at room temperature do not overlap (see Fig. 6a).

5. Conclusions

A solar cell with the GaAs world record layer structure containing an $(Al_{0.4}Ga_{0.6})_{0.52}In_{0.48}P$ BSF and a grid suited for high irradiance levels produced regular $I(V)$ and $V_{mp}(T)$ behavior at an irradiance of 1 sun. High irradiance *IV*-measurements on this cell revealed an unusual characteristic: with increasing irradiance an anomaly appeared in the high-voltage section of the *IV*-curve, indicating the presence of an energy barrier in the cell. A temperature dependence study of the anomaly at an irradiance of 55 suns revealed that it disappears at sufficiently high temperatures. A plot of the associated $V_{mp}(T)$ curve did not show the usual linear decrease with increasing temperature, but instead showed an increase at lower temperatures followed by a decrease after reaching a certain maximum.

The fact that a similar cell with higher doped $Al_{0.2}Ga_{0.8}As$ instead of $(Al_{0.4}Ga_{0.6})_{0.52}In_{0.48}P$ back surface field does not show the anomaly indicates that the phenomena reported here are closely related to the base/BSF valence band energy barrier and/or BSF doping level. These findings are in line with recently reported results on GaAs cells with GaInP back surface fields which indicates that any GaAs cell with an insufficiently doped, lattice-matched AlGaInP compound BSF will display anomalies under high irradiance.

The current transport across the base/BSF energy barrier is generally thought to be governed by thermionic emission and this indeed explains the exponential temperature dependence of the current through the barrier. However, the thermionic emission theory does not predict the observed irradiance dependence of the energy barrier's *IV*-characteristic. Therefore, subsequent research is required to fully understand the mechanism behind this energy barrier.

Acknowledgments

The authors would like to thank J.M. Olson at NREL for his useful suggestions. This work was financially supported by the Dutch Technology Foundation (STW) under project no. 07452.

References

[1] J.J. Schermer, P. Mulder, G.J. Bauhuis, M.M.A.J. Voncken, J. van Deelen, E. Haverkamp, P.K. Larsen, Epitaxial Lift-Off for large area thin film III/V devices, Physica Status Solidi (a) 202 (2005) 501–508.
[2] J.J. Schermer, G.J. Bauhuis, P. Mulder, E.J. Haverkamp, J. van Deelen, A.T.J. van Niftrik, P.K. Larsen, Photon confinement in high-efficiency, thin-film III–V solar cells obtained by epitaxial lift-off, Thin Solid Films 511–512 (2006) 645–653.
[3] G.J. Bauhuis, P. Mulder, E.J. Haverkamp, J.C.C.M. Huijben, J.J. Schermer, 26.1% thin-film GaAs solar cell using epitaxial lift-off, Solar Energy Materials and Solar Cells 93 (2009) 1488–1491.
[4] M.A. Green, K. Emery, Y. Hishikawa, W. Warta, Solar cell efficiency tables (version 33), Progress in Photovoltaics: Research and Application 17 (2009) 85–94.
[5] M.A. Green, Solar Cells: Operating Principles, Technology, and System Applications, Prentice-Hall, Englewood Cliffs, USA, 1982.
[6] A. Luque, S. Hegedus (Eds.), Handbook of Photovoltaic Science and Engineering, Wiley, Chichester, West Sussex, UK, 2003.
[7] W. Guter, A.W. Bett, $I-V$ characterization of tunnel diodes and multijunction solar cells, IEEE Transactions on Electron Devices 53 (2006) 2216–2222.
[8] M.O. Watanabe, Y. Ohba, Interface properties for GaAs/InGaAlP heterojunctions by the capacitance-voltage profiling technique, Applied Physics Letters 50 (1987) 906–908.
[9] B. Galiana, I. Rey-Stolle, M. Baudrit, I. García, C. Algora, A comparative study of BSF layers for GaAs-based single-junction or multijunction concentrator solar cells, Semiconductor Science and Technology 21 (2006) 1387–1392.
[10] J.M. Olson, M.A. Steiner, A. Kanevce, Using measurements of fill factor at high irradiance to deduce heterobarrier band offsets, in: Proceedings of the 37th Photovoltaic Specialists Conference, Hawaii, 2011. Preprint available at ⟨www.nrel.gov/docs/fy11osti/50737.pdf⟩.
[11] S.M. Sze, Physics of Semiconductor Devices, second ed., Wiley, New York, USA, 1981.